Nanoscale Res Lett (2010) 5:1836–1840
DOI 10.1007/s11671-010-9721-z

NANO EXPRESS

Atomic Layer Deposition of ZnO on Multi-walled Carbon Nanotubes and Its Use for Synthesis of CNT–ZnO Heterostructures

X. L. Li · C. Li · Y. Zhang · D. P. Chu · W. I. Milne · H. J. Fan

Received: 7 June 2010 / Accepted: 26 July 2010 / Published online: 7 August 2010

Abstract In this article, direct coating of ZnO on PECVD-grown multi-walled carbon nanotubes (MWCNTs) is achieved using atomic layer deposition (ALD). Transmission electron microscopy investigation shows that the deposited ZnO shell is continuous and uniform, in contrast to the previously reported particle morphology. The ZnO layer has a good crystalline quality as indicated by Raman and photoluminescence (PL) measurements. We also show that such ZnO layer can be used as seed layer for subsequent hydrothermal growth of ZnO nanorods, resulting in branched CNT–inorganic hybrid nanostructures. Potentially, this method can also apply to the fabrication of ZnO-based hybrid nanostructures on other carbon nanomaterials.

Keywords ZnO · Atomic layer deposition · Carbon nanotubes · Hybrid nanomaterials · Hydrothermal · Solar cells

Introduction

Carbon nanotube (CNT) and inorganic composite materials have attracted much attention recently due to their potential application such as in photocatalyst, gas sensors, supercapacitors, and field emission devices [1]. It has been reported that the optical and electrical properties of CNT–inorganic composites can be enhanced compared to the individual constituents [2]. For example, CNT films when employed as conducting scaffolds in a TiO_2 based photoelectrochemical cell showed an enhancement of the photoconversion efficiency by a factor of two [3].

CNT–ZnO represents one of most important members of the CNT–inorganic composites family due to the fact that ZnO is a n-type semiconductor with a direct wide band gap (3.37 eV) and large exciton binding energy (60 meV) [4]. For instance, an ultrafast nonlinear optical switching behavior has been observed from ZnO-coated CNTs [5]. The coaxial heterostructured nanotubes with a p-channel CNT combined with an n-channel ZnO shell may be integrated into logical inverters [6].

Various synthesis strategies based on physical and chemical process toward CNT–inorganic hybrids have been established so far, as summarized in recent review articles [1, 7]. ALD is a cyclic self-limiting deposition method, which is capable of conformal and uniform coating of thin films at the atomic level. It has been applied to deposit a variety of materials including oxides and metals on various nonplanar high-aspect-ratio substrates [8]. ALD on CNTs has been an interesting topic, but there are relatively few reports compared to ALD on inorganic or polymers nanostructures. ALD coating CNTs with continuous amorphous Al_2O_3 layers has been reported by Kim et al. [9]. However, as for direct ALD ZnO on CNTs, the so far available reports show only ZnO nanoparticles or morphological poor-defined ZnO layer. While such poorly-defined tube–particle structure is shown useful for field emission applications [10, 11], more homogeneous coatings are desirable for CNT-based photonic devices. Kim et al. [12] achieved relatively smooth ZnO coating on CNT using a thin ALD alumina buffer layer. However, the

X. L. Li · H. J. Fan (✉)
Division of Physics and Applied Physics, School of Physical and Mathematical Sciences, Nanyang Technological University, 21 Nanyang Link, Singapore 637371, Singapore
e-mail: fanhj@ntu.edu.sg

C. Li · Y. Zhang · D. P. Chu · W. I. Milne
Electrical Engineering Division, Engineering Department, University of Cambridge, 9 JJ Thomson Avenue, CB3 0FA Cambridge, UK

existence of an Al_2O_3 buffer layer breaks the direct contact of ZnO to the CNTs and thus prevents the charge transfer, a process needed for the functions of photoelectrochemical cells. Furthermore, the low optical quality of such ZnO layers, as seen from the weak UV emission, will hinder the photonic application of such hybrid nanostructures [12].

In this work, we report the direct ALD of ZnO on vertical-aligned multi-walled carbon nanotube arrays. The resulting ZnO layers have a well-defined morphology and higher smoothness compared to the discontinuous nanoparticles in previous reports. We also demonstrate that the deposited ZnO layer can be used as a seed layer for the hydrothermal growth of ZnO nanorods. This provides a new method for the fabrication of CNT–ZnO three-dimensional (3-D) hybrid nanostructures, which might be useful as photoelectrochemical anode materials. The PL properties of the ZnO-coated CNTs and CNT–ZnO 3-D nanotrees will be discussed.

Experiment Details

The vertical-aligned MWCNT arrays were grown by plasma-enhanced chemical vapor deposition (PECVD) reported elsewhere [13]. ALD of ZnO was conducted using a Beneq system (TFS 200) at 200°C using diethylzinc ($Zn(C_2H_5)_2$, DEZ) and water as the zinc and oxygen source, respectively. High purity N_2 was the process gas in our experiment. During the deposition, the reaction chamber was maintained at 1.0 mbar with a steady N_2 steam at 200 SCCM (cubic centimeter per minute). Each ALD cycle consisted of a 250-ms precursor pulse and 10-s purging time with N_2. The relatively short precursor exposures and long purging times were adopted in order to achieve uniform coatings on the closely stacked CNTs arrays. The shell thickness was controlled by the numbers of the ALD cycles. A typical deposition consists of 80 cycles. For ALD of alumina (Al_xO_y), trimethylaluminum [$Al(CH_3)_3$] and water were used as aluminum and oxygen source, respectively. A thickness of 7 nm was obtained from 60 cycles.

ZnO nanorods growing on vertical-aligned MWCNTs were synthesized using the standard hydrothermal method. The ALD ZnO-coated CNTs substrate was immersed into a 35-mL aqueous solution of equimolar zinc nitrate [$Zn(NO_3)_2{\cdot}6H_2O$] and hexamethylenetetramine ($C_6H_{12}N_4$) in an autoclave. The reaction was conducted at 95°C for 5 h. After reactions, the substrate was removed from the solution, rinsed with deionized water, and dried with N_2.

The morphology of the as-fabricated samples was characterized using a JEOL JSM-6700F field emission scanning electron microscope (FESEM) and a JEOL JEM-1400F transmission electron microscope (TEM). PL and Raman measurements were taken with a Renishaw system using 325- and 532-nm laser as the excitation source, respectively.

Results and Discussion

Figure 1a shows the TEM image of the typical morphology of the PECVD CNTs prior to deposition. Most of the nanotubes are multiwall tubes, and the average diameter of the CNTs is about 7 nm. Figure 1b shows the typical TEM image of ALD ZnO-coated CNTs. Clearly, the deposited ZnO shell is continuous and uniform along the tube. The ZnO shell thickness is about 18 nm, corresponding to a growth rate of 0.22 nm per cycle. This value is in consistent with the regular ALD ZnO process [14–16]. Figure 1d and e show the SEM images of the ZnO-coated aligned CNTs. As can be seen, the ALD process did not affect the overall alignment of the CNTs and that CNTs on the whole substrate area were coated with a ZnO shell. For comparison, the result of direct ALD of 7 nm Al_xO_y on the same CNTs is also shown in Fig. 1e. As expected, the amorphous Al_xO_y layer exhibits long range continuity and smoothness. The growth rate of Al_xO_y is 0.13 nm per cycle, which is consistent with the previous report [16].

There are several factors that affect the morphology of the ALD ZnO shell on CNTs. The first one is the surface configuration of the CNTs. As a micromolecular form of carbon, CNT can be regarded as graphitic layers (sp^2-hybridized carbon atoms) rolled up into a cylindrical form. A perfect CNT is chemically inert. However, there generally exist defects on the tube wall, such as bending in the nanotube, the finite size of crystalline domains, sp^3-hybridized bonds, or functional groups created by oxidation [17, 18]. These defects or functional groups make the CNT surface reactive to the atomic species of an ALD precursor. The Raman spectrum of our PECVD MWCNTs (Fig. 2 curve a) shows a strong D band, indicating the existence of defects on the tube wall. Compared to MWCNTs, the surfaces of the single-walled carbon nanotubes (SWCNTs) are known to have less structural defects or impurity sites on the tube walls. This is the reason why ALD on SWCNTs is generally more challenging than on MWCNTs. The same argument holds true for deposition on graphene. In the ALD work by Min et al. [10], ZnO particles were deposited on the SWCNTs. It is most likely that the nanoparticles were formed selectively on the defective sites or impurities on the nanotubes wall, which provide chemisorptions sites for DEZ molecules.

The second factor is the ALD processing parameters. It is known that one ALD cycle consists of two half-chemical reactions. After each-half cycle, the excess precursor needs to be thoroughly purged out; otherwise, it will contribute to

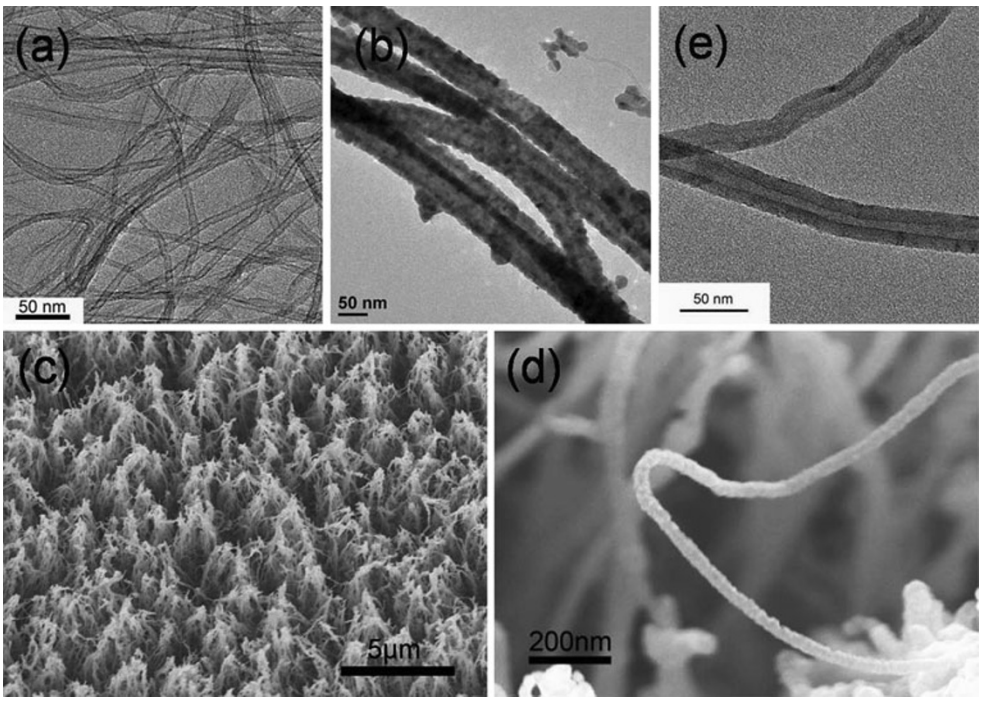

Fig. 1 **a** TEM image of PECVD-grown CNTs. **b** TEM image of ALD ZnO-coated CNTs. **c** and **d** SEM images of ALD ZnO-coated CNTs. **e** TEM image of ALD Al_xO_y-coated CNTs

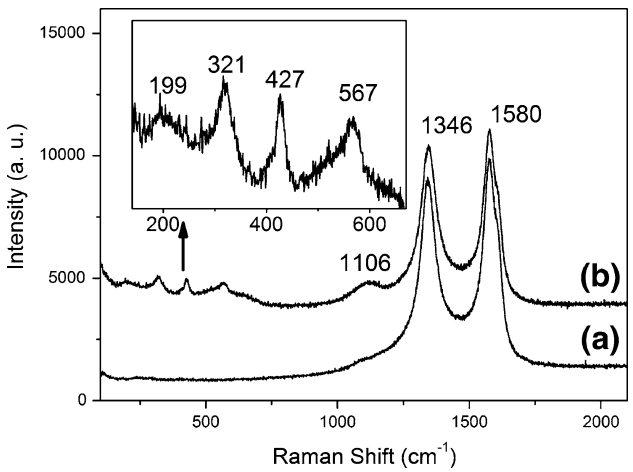

Fig. 2 Raman spectrum of CNTs before (**a**) and after (**b**) ALD of ZnO. *Inset*: Raman spectrum in the range of 150–650 cm^{-1} of ZnO-coated CNTs

a chemical vapor deposition (CVD) reaction. With the occurrence of CVD reactions, the growth rate will be higher than a regular ALD process. In our experiment, to exclude the unwanted CVD reaction, we used short precursor exposures and long purging times. The growth rate of ALD ZnO, 0.22 nm/cycle, in our experiment is comparable to the previously reports based on DEZ and water [14, 15], indicating that there is negligible CVD reaction in our case. Furthermore, the alignment of CNTs also matters. Note that in Ref. [11] and [12], the authors used randomly oriented MWCNTs for ZnO ALD. Compared to the vertical-aligned CNTs in our cases, there is much less free space between the tubes, which makes the purge of the excess ALD precursors after each semi-cycle difficult. Subsequently, additional CVD reactions may occur. This could explain why only poor-defined ZnO agglomerates were observed on CNTs in previous work [11, 12]. It is also noted that the growth rate (0.35 nm/cycle) was much higher than the regular ALD process (0.22 nm/cycle), further implying the occurrence of additional CVD reactions in their experiment [12]. In our experiment, we used vertical-aligned MWCNTs and a longer purge time to exclude possible CVD reactions. This contributes to the improved conformity of ALD ZnO.

Lastly, ZnO tends to crystallize and texture along *c*-orientation even at low temperatures. As predict from the first-principle simulations, an uncompensated polarity exists in ultrathin ZnO films [19]. The involvement of the polarity of ZnO nanoclusters during the ALD explains why the ZnO shells are not as smooth as the amorphous Al_xO_y on CNT, as seen from the TEM image (Fig. 1e) and previous reports [9, 12].

Raman spectrum of CNTs prior to (curve a in Fig. 2) and after (curve b in Fig. 2) ALD ZnO were measured. As seen, a G band appears at about $\sim$1580 cm^{-1} corresponding to sp^2-hybridized carbon and a D band at $\sim$1346 cm^{-1} originating from disordered carbon [17, 18]. In addition to the D band, the D′ band as a shoulder of the

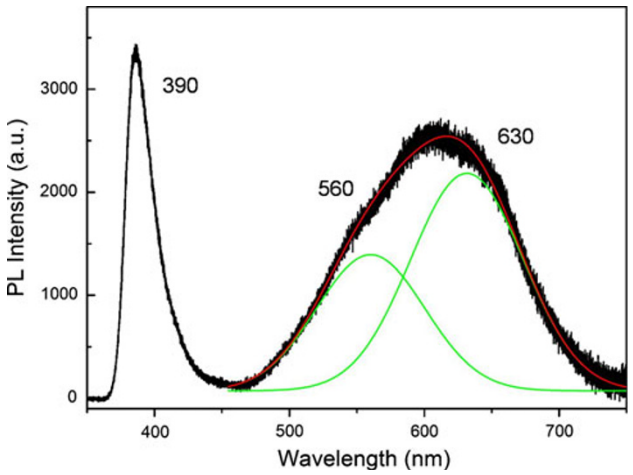

Fig. 3 Room-temperature PL spectra of ALD ZnO-coated CNTs

G band appears at about 1614 cm^{-1}, which also originates from the disorder features due to the finite size effect of the crystalline domain or lattice distortion [18]. The intensity ratio of the D′ over the G band ($I_{D'}/I_G$) increases with a decrease in the graphite crystalline domain. The D band and D′ band peak are very strong, indicating that the CNTs we used have considerable number of defects on the surface. After ALD ZnO those D band, D′ band and G band peaks changed only slightly. Additional Raman peaks from the ZnO shells appeared; the relatively strong peaks at 427 and 567 cm^{-1} correspond to E_2^{high} and A_1 (LO) modes, respectively, and the peaks at 199, 321, and 1106 cm^{-1} are attributed to $2E_2^{low}$, $E_2^{high}-E_2^{low}$, and 2LO, respectively. These Raman peaks are consistent with the previous reports [20].

Figure 3 shows the room-temperature PL spectrum of ALD ZnO-coated CNTs, in which the UV emission peak at about 390 nm (3.18 eV) corresponds to the near-band-edge emission of ZnO crystal. An intensive broad visible emission due to defects or impurities is also observed. It appears to be a superposition of two main components at ~560 and ~630 nm, a feature similar to the PL of ZnO nanowire reported by Fan et al. [21]. Emission in the green spectra range is commonly observed in bulk and nanostructure ZnO and the origin is still under debate [22, 23]. The orange–red emission is generally associated with oxygen interstitial [24]. Compared to the only available report so far on PL of ALD ZnO [12], the UV to visible emission ratio of our sample is significantly higher. That might be due to the high crystalline quality of the ZnO shell in our case.

Low-temperature hydrothermal growth is a popular method for synthesizing ZnO nanorods on any type of substrates. Based on hydrothermal growth of ZnO on nanostructured substrates, hierarchical heterogeneous nanowires can be realized [25–27]. A prerequisite for ZnO hydrothermal growth of nanorods is the seed layer, and the quality of the seed layer (e.g., crystallinity, smoothness, orientation). Here, we demonstrate that the deposited ZnO shell can also be used as seed layer for hydrothermal growth of ZnO nanorods on CNTs, without any further annealing process. Figure 4a shows the schematics of the growth processes of the CNT–ZnO 3-D hybrid structure. Figure 4b shows the SEM images of the synthesized CNT–ZnO 3-D hybrid structure. The densely packed ZnO nanorods are aligned roughly perpendicularly to the axis of the tubes. The size of the branched ZnO nanorods is about 30 nm in the diameter and several hundred nm in length.

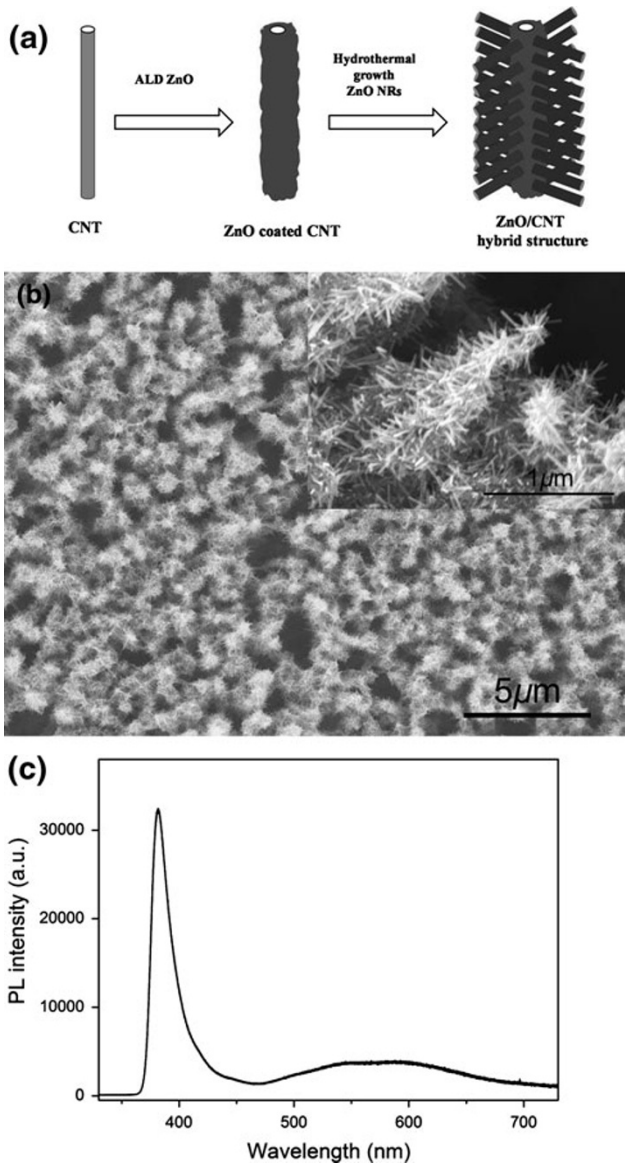

Fig. 4 **a** Schematics of the growth process, **b** SEM image, and **c** PL spectrum of the CNT–ZnO branched nanostructure. *Inset*: magnified SEM image

Figure 4c shows the room-temperature PL spectrum of CNT–ZnO 3-D hybrid structure. It shows a strong UV peak

positioned at 385 nm with full width at half maximum (FWHM) of about 21 nm and a low and broadened peak in the visible range. This is consistent with the generally obtained PL spectra of ZnO nanorods growth by hydrothermal methods [27]. Compared with the ALD ZnO seed layer on CNTs, the UV emission intensity and the ratio of UV/Visible peak of the CNT–ZnO 3-D hybrid structure are much higher. This is not surprising as the ZnO nanorods are single crystalline, while the ALD ZnO is a polycrystalline thin layer.

Conclusion

Direct ALD of ZnO thin layers on PECVD-grown CNTs has been successfully achieved without pretreatment of the CNTs. The deposited ZnO shell is continuous and uniform along the tube long axis. Raman and PL studies reveal that the ZnO shells are of reasonably good crystalline quality, in contrast to the ALD ZnO shell on CNTs through an Al_2O_3 buffer layer in the previous report. Also we have demonstrated that the ALD ZnO can be used as seed layer for hydrothermal growth of ZnO nanorods on CNTs, forming a CNT–ZnO 3-D hybrid nanostructure, which could be useful materials for electronic or energy-related applications.

References

1. D. Eder, Chem. Rev. **110**, 1348 (2010)
2. J.M. Haremza, M.A. Hahn, T.D.K.S. Chen, J. Calcines, Nano. Lett. **2**, 1253 (2002)
3. A. Kongkanand, R.M. Domínguez, P.V. Kamat, Nano. Lett. **7**, 676 (2007)
4. J. Zhong, A.H. Kitai, P. Mascher, W. Puff, J. Electrochem. Soc. **140**, 3644 (1993)
5. Y.W. Zhu, H.I. Elim, Y.L. Foo, T. Yu, Y.J. Liu, W. Ji, J.Y. Lee, Z.X. Shen, A.T.S. Wee, J.T.L. Thong, C.H. Sow, Adv. Mater. **18**, 587 (2006)
6. R. Martel, T. Schmidt, H.R. Shea, T. Hertel, P. Avouris, Appl. Phys. Lett. **73**, 2447 (1998)
7. D. Tasis, N. Tagmatarchis, A. Bianco, M. Prato, Chem. Rev. **106**, 1105 (2006)
8. M. Knez, K. Nielsch, L. Niinistö, Adv. Mater. **19**, 3425 (2007)
9. J.S. Lee, B. Min, K. Cho, S. Kim, J. Park, Y.T. Lee, N.S. Kim, M.S. Lee, S.O. Park, J.T. Moon, J. Cryst. Growth **254**, 443 (2003)
10. Y.S. Min, E.J. Bae, J.B. Park, U.J. Kim, W. Park, J. Song, C.S. Hwang, N. Park, Appl. Phys. Lett. **90**, 263104 (2007)
11. J.M. Green, L. Dong, T. Gutu, J. Jiao, J.F. Conley Jr, Y. Ono, J. Appl. Phys. **99**, 094308 (2006)
12. D.S. Kim, M.S. Lee, R. Scholz, M. Knez, U. Gösele, J. Fallert, H. Kalt, M. Zacharias, Appl. Phys. Lett. **93**, 103108 (2008)
13. S. Hofmann, M. Cantoro, B. Kleinsorge, C. Casiraghi, A. Parvez, J. Robertson, C. Ducati, J. Appl. Phys. **98**, 034308 (2005)
14. A.W. Ott, R.P.H. Chang, Mater. Chem. Mater. Phys. **58**, 132 (1999)
15. E. Guziewicz, I.A. Kowalik, M. Godlewski, K. Kopalko, V. Osinniy, A. Wojcik, S. Yatsunenko, E. Lusakowska, W. Paszkowicz, M. Guziewicz, J. Appl. Phys. **103**, 033515 (2008)
16. J.W. Elam, S.M. George, Chem. Mater. **15**, 1020 (2003)
17. W.Z. Li, H. Zhang, C.Y. Wang, Y. Zhang, L.W. Xu, K. Zhu, S.S. Xie, Appl. Phys. Lett. **70**, 2684 (1997)
18. A. Hirsch, Angew. Chem. Int. Ed. **41**, 1853 (2002)
19. J. Goniakowski, C. Noguera, L. Giordano, Phys. Rev. Lett. **98**, 205701 (2007)
20. R. Cuscó, E. Alarcón-Lladó, J. Ibáñez, L. Artús, J. Jiménez, B. Wang, M.J. Callahan, Phys. Rev. B **75**, 165202 (2007)
21. H.J. Fan, R. Scholz, F.M. Kolb, M. Zacharias, Appl. Phys. Lett. **85**, 4142 (2004)
22. A.B. Djurisic, Y.H. Leung, Small **2**, 944 (2006)
23. M.D. McCluskey, S.J. Jokela, J. Appl. Phys. **106**, 13 (2009)
24. F.H. Leiter, H.R. Alves, A. Hofstaetter, D.M. Hofmann, B.K. Meyer, Phys. Status Solidi B **226**, R4 (2001)
25. S.A. Studenikin, N. Golego, M. Cocivera, J. Appl. Phys. **84**, 2287 (1988)
26. W.D. Zhang, Nanotechnology **17**, 1036 (2006)
27. C.W. Cheng, B. Liu, H.Y. Yang, W.W. Zhou, L. Sun, R. Chen, S.F. Yu, J.X. Zhang, H. Gong, H.D. Sun, H.J. Fan, ACS NANO **3**, 3069 (2009)